Cryo-EM structure of SNAP-SNARE assembly in 20S particle

Qiang Zhou^{1,*}, Xuan Huang^{1,*}, Shan Sun^{1,*}, Xueming Li², Hong-Wei Wang², Sen-Fang Sui¹

¹State Key Laboratory of Biomembrane and Membrane Biotechnology, Center for Structural Biology, School of Life Sciences, Tsinghua University, Beijing 100084, China; ²Ministry of Education Key Laboratory of Protein Science, Center for Structural Biology, Tsinghua-Peking Joint Center for Life Sciences, School of Life Sciences, Tsinghua University, Beijing 100084, China

N-ethylmaleimide-sensitive factor (NSF) and α soluble NSF attachment proteins (α -SNAPs) work together within a 20S particle to disassemble and recycle the SNAP receptor (SNARE) complex after intracellular membrane fusion. To understand the disassembly mechanism of the SNARE complex by NSF and α -SNAP, we performed single-particle cryo-electron microscopy analysis of 20S particles and determined the structure of the α -SNAP-SNARE assembly portion at a resolution of 7.35 Å. The structure illustrates that four α -SNAPs wrap around the single left-handed SNARE helical bundle as a right-handed cylindrical assembly within a 20S particle. A conserved hydrophobic patch connecting helices 9 and 10 of each α -SNAP forms a chock protruding into the groove of the SNARE four-helix bundle. Biochemical studies proved that this structural element was critical for SNARE complex disassembly. Our study suggests how four α -SNAPs may coordinate with the NSF to tear the SNARE complex into individual proteins.

Keywords: α-SNAP; NSF; cryo-EM; 20S particle; membrane fusion *Cell Research* (2015) **25**:551-560. doi:10.1038/cr.2015.47; published online 24 April 2015

Introduction

As the central player in membrane fusion, the SNAP receptor (SNARE) proteins consist of v-SNAREs on vesicle membranes and t-SNAREs on target membranes. During membrane fusion, SNARE proteins on opposing membranes coil together to form a highly stable four-helix bundle complex with conserved leucine-zipper-like layers embedding an ionic zero-layer at the center [1-6]. The SNARE complex is believed to be the minimum machinery necessary to drive membrane fusion [7]. The synaptic SNARE complex, as a classical family of SNARE complexes, comprises one v-SNARE (VAMP, also called synaptobrevin) and two t-SNAREs (syntaxin and SNAP25) [8]. After membrane fusion, the stable SNARE complexes must be disassembled into individual SNARE proteins for reuse. α soluble NSF attachment proteins (α-SNAPs) and N-ethylmaleimide-sensitive factor (NSF) bind sequentially to the SNARE complex to form a complex, termed 20S particle, which is responsible for disassembling the SNARE complex [9-11]. In the 20S particle, NSF hydrolyzes ATP into ADP and phosphate, and utilizes the hydrolysis energy to disassemble SNARE complexes, which requires its interaction with α -SNAP molecules [10, 12].

NSF is a ring-shaped homo-hexameric protein, with each protomer consisting of an N-terminal domain (N-domain) and two ATP-binding domains D1 and D2 [13-15]. D2 domain is responsible for maintaining NSF as a hexamer, while D1 domain is catalytically active and functions to hydrolyze ATP accompanied by a major conformational change of itself as well as the N-domain attached to it [16-18]. Previous studies indicated that the N-domain of NSF interacts with the C-terminal end of α-SNAP, which mediates the interaction of NSF and the SNARE complex [19-23]. Crystallographic study has revealed the structure of Sec17, a yeast homolog of α-SNAP, composed of an N-terminal twisted sheet of α -helical hairpins and a C-terminal α -helical bundle [24]. The positively charged residues in the concave surface of the N-terminal sheet of α -SNAP were shown to be involved in the interaction with the SNARE complex [25]. Despite extensive studies of the structures of NSF, α-SNAP and the SNARE complex individually, how the SNARE complex is disassembled in the 20S particle,

Correspondence: Sen-Fang Sui^a, Hong-Wei Wang^b

Received 29 January 2015; revised 25 February 2015; accepted 17 March 2015; published online 24 April 2015

^{*}These three authors contributed equally to this work.

^aE-mail: suisf@mail.tsinghua.edu.cn

^bE-mail: hongweiwang@tsinghua.edu.cn



however, is still enigmatic due to the limited structural information for the entire 20S particle [17, 26-28].

In this study, we used single-particle cryo-electron microscopy (cryo-EM) analysis to determine the structure of the 20S particle and reconstructed the structure of $\alpha\text{-SNAP-SNARE}$ assembly portion in the 20S particle at a resolution of 7.35 Å. This structure reveals an unexpected assembly in which four $\alpha\text{-SNAPs}$ form a right-handed assembled barrel wrapping around the single left-handed SNARE within a 20S particle. A conserved hydrophobic tip of $\alpha 9/\alpha 10$ helix hairpin of each $\alpha\text{-SNAP}$ was found to protrude into the groove of the SNARE four-helix bundle like a chock. Our structural and biochemical analysis provides new insights into the mechanism by which four $\alpha\text{-SNAPs}$ disassemble the SNARE complex.

Results

Cryo-EM of the 20S particle

To understand the mechanism of SNARE disassembly in the 20S particle, we previously reconstituted 20S particles with a quality suitable for EM structural analysis [17]. The reconstituted 20S particles, in an NP40-containing buffer solution, had full SNARE assembly activity but showed partial aggregation with their SNARE ends attaching to detergent micelles as observed under EM (Supplementary information, Figure S1A-S1C). Despite the partial aggregation, we obtained cryo-EM images of individual 20S particles in a frozen-hydrated specimen (Supplementary information, Figure S1D) and performed two-dimensional (2D) single-particle analysis of them. The 2D class averages of these particles correspond mainly to the top view of 20S particles (Supplementary information, Figure S1E). Astoundingly, a square-shaped density feature surrounding a small circle with high intensity exists in almost all of the top-view 2D class averages (Figure 1D and Supplementary information, Figure S1E). Superimposed over the rather blurred hexameric shape in the larger radii, the square-shaped structure appears to be composed of four discrete units assembling around a circular structure in a four-fold symmetry (Supplementary information, Figure S1F). This strongly suggests that the α -SNAP assembly on the top of the NSF hexameric ring in a 20S particle forms a tetramer.

To further investigate the structure of the 20S particle in three dimensions (3D), we needed to solve the problems of particle aggregation and top-view preferential orientation. Using the lipid nanodisc technology [29-32], we successfully reconstituted functional 20S particles with the transmembrane helix of SNARE complex's VAMP protein integrated into the nanodisc (Supple-

mentary information, Figure S2A and S2B). These nanodisc-tethered 20S (ND-20S) particles behaved much better than mono-dispersed molecules under EM for both negatively stained and frozen-hydrated specimens (Figure 1A and Supplementary information, Figure S2C). As most ND-20S particles adopted a side-view orientation on a thin carbon film in vitreous ice, the major feature of the ND-20S particle, i.e., the D1 and D2 rings of NSF sit at one end as a two-layered density and the oval-shaped nanodisc density attaches to the other end, can be clearly identified in raw particle images and 2D class averages (Figure 1B). Although very few, some top-view images of the ND-20S particle in the frozen-hydrated specimen can be aligned and summed up into 2D class averages, showing almost the same feature as in the top-view 2D class averages of the 20S particles in NP40 solution. This indicates that the overall composition and architecture of the 20S particle is preserved in different means of reconstitution. 3D reconstruction from the negatively stained ND-20S particles generated a map with a similar overall shape to our previously reconstructed 20S particle [17], but having an addition cap density of the nanodisc on the top (Supplementary information, Figure S2D).

Using the map of negatively stained ND-20S particle as an initial model, we performed 3D reconstruction of the vitrified ND-20S particles and obtained a 3D map with an overall resolution of ~13 Å (Supplementary information, Figure S2E-S2H). This structure, without any symmetry imposed, showed a clearly hexameric structure of the NSF D1-D2 double ring at the bottom and the α-SNAP-SNARE assembly sitting on top of the NSF hexamer. In contrast, neither the symmetry nor the detailed feature of the α-SNAP-SNARE assembly can be clearly defined. Closer examination of the 2D class averages and 3D reconstruction of the vitrified ND-20S particles revealed a relative tilting of ~10° between the α-SNAP-SNARE assembly and the D1-D2 hexameric ring assembly (Figure 1B and Supplementary information, Figure S2F). We reasoned that the possible symmetry mismatch and flexibility between the α-SNAP-SNARE assembly and the NSF hexamer may prevent obtaining a higher resolution reconstruction of the entire 20S particle.

20S particle segmentation and 3D reconstruction of the α -SNAP-SNARE assembly

The D1-D2 model segmented from the low-resolution reconstruction of the entire 20S particle shows very similar features to our previous 3D reconstruction of the NSF in the ATP state [17], allowing us to segment the upper part of each 20S particle image by subtracting the NSF D1-D2 ring density from the raw image and perform sin-

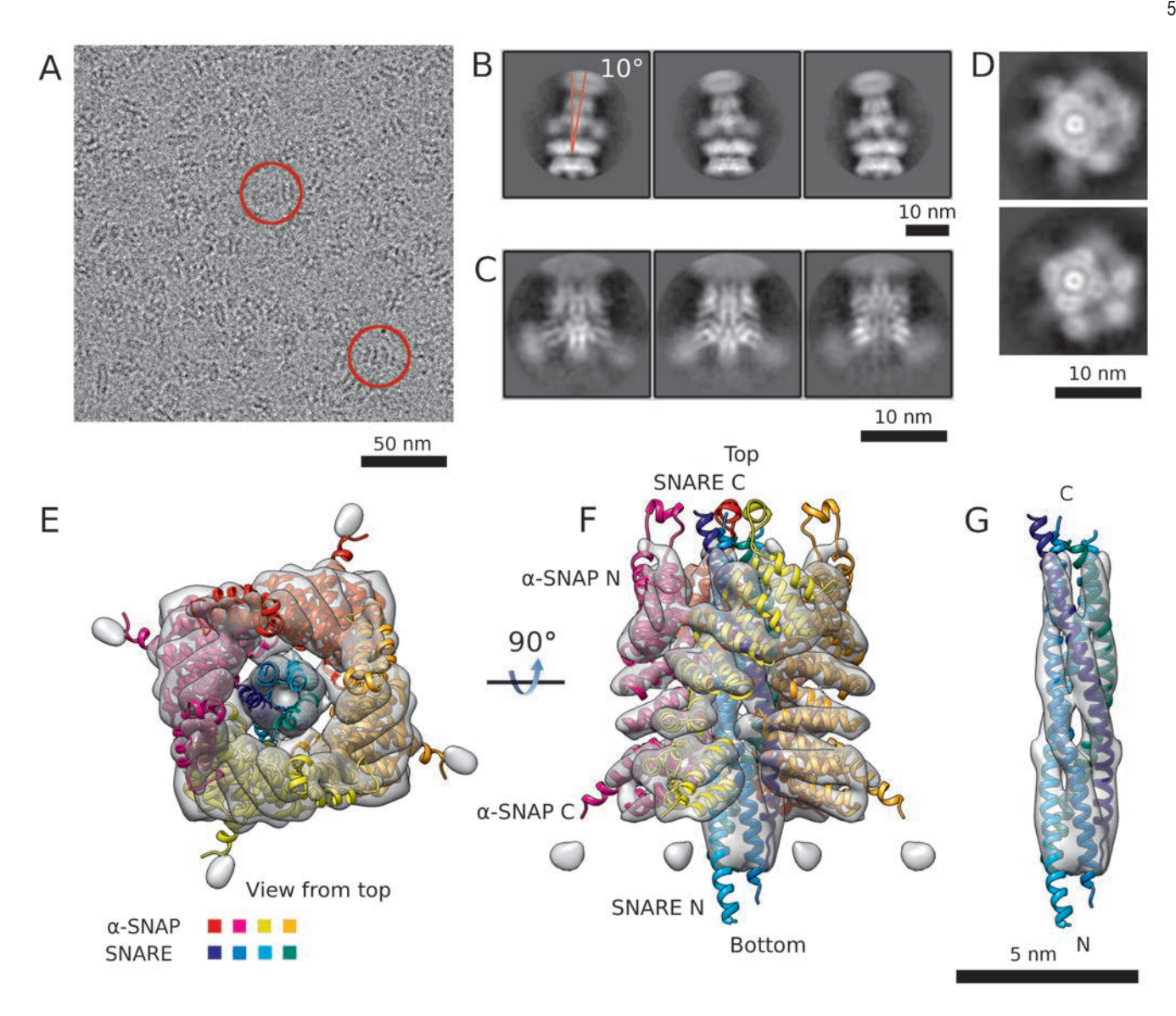


Figure 1 Cryo-EM 3D reconstruction and atomic model docking of the upper part of ND-20S. (A) A representative micrograph of vitrified ND-20S particles with typical particles marked by red circles. (B) Typical 2D class averages of ND-20S. The relative tilt between the upper part and lower parts of the complex is labeled in the first class average. (C) Typical 2D class averages of the upper portion of ND-20S. (D) Typical 2D class averages of 20S particle in the top view. (E) Top and (F) side views of the ND-20S upper part 3D map docked with atomic models of α-SNAP and SNARE complex shown in different colors for clarity. (G) Docking of atomic model of the SNARE complex in the central portion of the 3D reconstruction.

gle-particle analysis of the resulted images (Supplementary information, Figures S3, S4 and Data S1) to overcome the flexibility difficulty. Indeed, this practice led to a much better defined 2D class averages of the upper part of the 20S particle with secondary structural elements clearly visible (Figure 1C). Immediately visible in these 2D class averages are the two long thread-like densities parallel to the central axis in the middle and additional densities attached to them at both sides in a mirrored symmetry. This is in agreement with the existence of a

four-fold symmetry in the assembly as revealed in the top-view 2D class averages. We then exploited 3D reconstruction of the segmented images as obtained above. We first generated a 3D initial model from the 2D class averages of these segmented images and the 2D class averages of 20S particles in the top view (Supplementary information, Figure S4D). Subsequently, we performed 3D refinement of the segmented images against the low-resolution initial model with a four-fold symmetry (the determination of four-fold symmetry was described

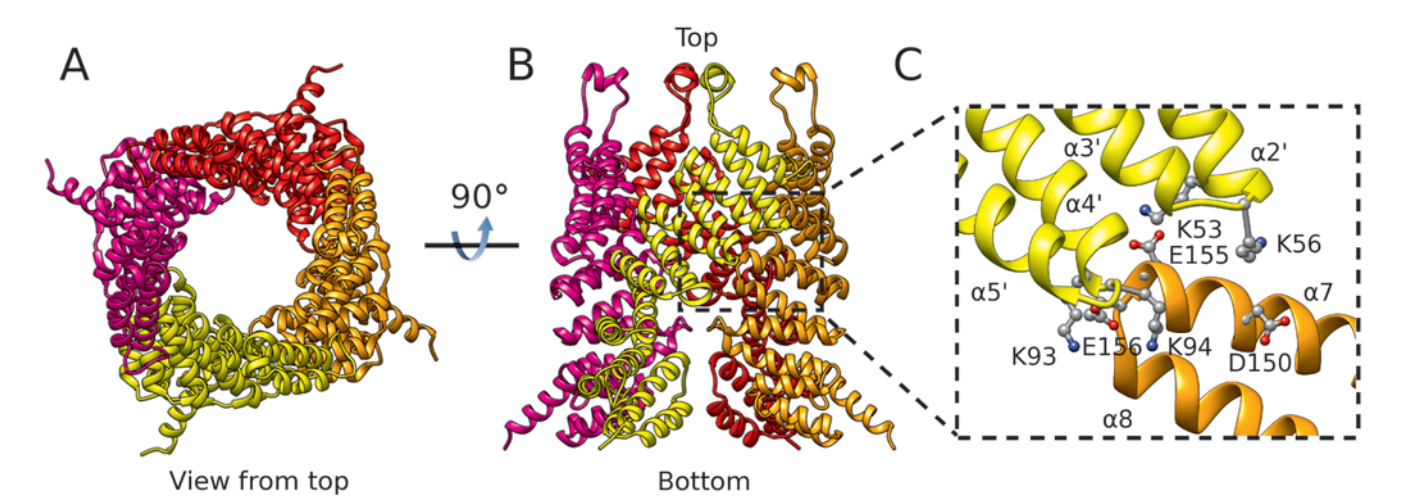


Figure 2 The interaction between α -SNAP protomers. (A) Top and (B) side views of atomic models of α -SNAP tetramer. (C) Enlarged view of the protomer interface with relevant charged residues labeled with ball and stick model. The helices are numbered according to the crystal structure in the two protomers.

in Supplementary information, Figure S4H) and obtained a 3D map at a resolution of 7.35 Å (Figure 1E-1G and Supplementary information, Figure S4E-S4G and Movie S1). In the map, major secondary structural elements in both α -SNAP protein and SNARE complex are clearly visible. Similar practices using other symmetries including C2, C3, C5 and C6 all failed to reconstruct 3D structure of the complex.

The well-defined features in the reconstruction of α-SNAP-SNARE assembly allowed us to unambiguously fit the homologous atomic models of four-helical bundle portion of the SNARE complex and α-SNAP protein as rigid bodies into the 3D map with high fidelity (Figure 1E-1G, and Supplementary information, Movie S1). Most α helices of α -SNAP are clearly visible in the map except for the very C-terminal end, near which there are weak densities possibly corresponding to the N-domain of NSF known to interact with α-SNAP's C terminus [19-23]. The four-helical bundle of the SNARE complex fits perfectly in the central left-handed four threadlike densities albeit with the side chain of each residue in the helix unsolved. However, the comparison of the diameter variation pattern between the atomic model of the SNARE complex and the EM density along their super-helical axis allowed us to estimate the layer positions in the complex (see discussion below and Supplementary information, Figure S5B).

Four α -SNAPs assemble into a barrel within the 20S particle

Within the 20S particle, four α -SNAPs assemble around the SNARE complex into a right-handed helical

cylindrical barrel (Figure 2A and 2B). The interaction between α-SNAPs mainly occurs at the N-terminal portion of the protein, while there is little interaction at the C-terminal part. The interaction interface between two adjacent α-SNAPs involves mainly negatively charged residues (D150, E155 and E156) of α 7 and α 8 helices in one protomer and positively charged residues (K53, K56, K93 and K94) of $\alpha 2' - \alpha 3'$ loop and $\alpha 4' - \alpha 5'$ loop in the adjacent protomer (Figure 2C). Such a highly electrostatically mediated interaction stabilizes the four α-SNAPs in a tight structure around the C-terminal region of the SNARE complex, a feature with a possible role in mediating both the α-SNAP-SNARE assembly at the early stage and the SNARE complex disassembly at the late stage in a cooperative manner during the SNARE disassembly cycle. Indeed, mutations of α-SNAP's key residues involved in the interaction abolish SNARE disassembly activity [25]. The lack of interactions between α-SNAPs at their C-terminal portion on the other hand may reflect the potential domain mobility of this portion induced by NSF-mediated ATP hydrolysis.

Interaction between α -SNAP and the SNARE complex

In our structure, each α -SNAP has four interaction sites with the SNARE complex from the top to the bottom (Figure 3A, 3B and Supplementary information, Figure S5). The two upper interaction sites and the very bottom interaction site are mostly on the outer surface of a SNARE helical strand, most likely via electrostatic interaction as predicted by the crystallographic structure of α -SNAP [24, 25]. Of particular interest is the third interaction site at the lower part with the most extensive

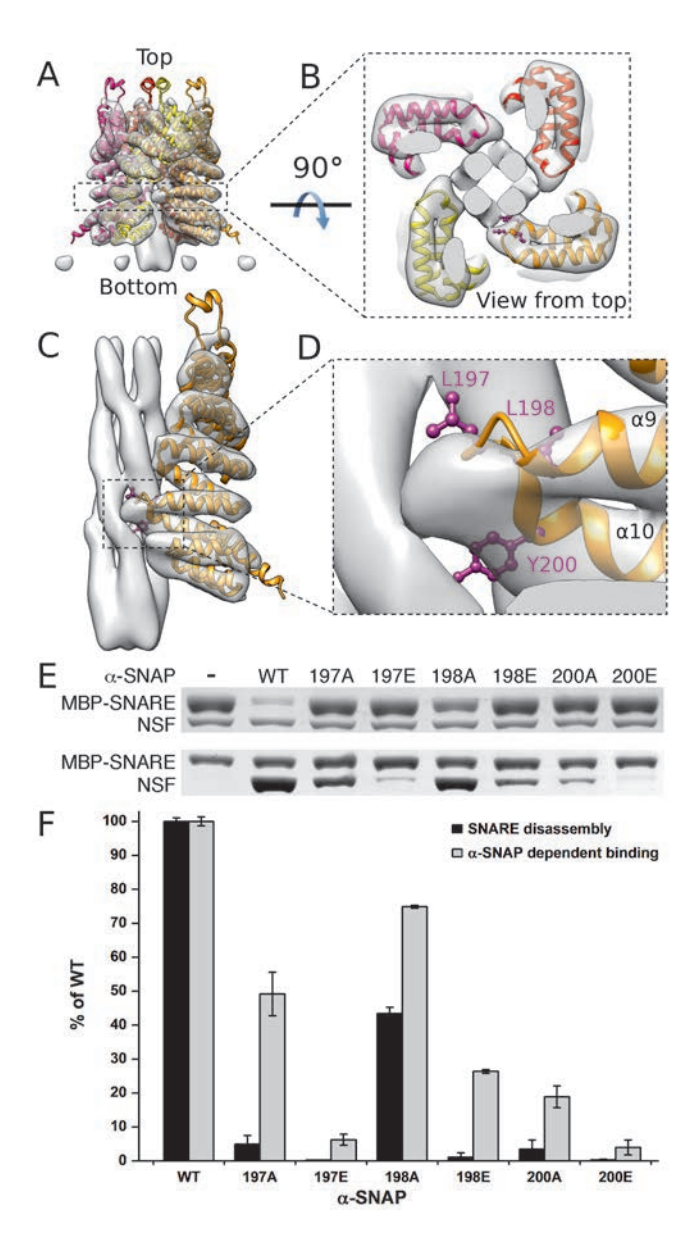


Figure 3 The helix hairpin tip of α -SNAP interacting with the SNARE complex. (A) Cryo-EM 3D map of the upper part of ND-20S docked with four α -SNAPs. (B) Top view of the marked slab in A. (C) Side view of the cryo-EM map docked with only one α -SNAP protomer, with the other three α -SNAP protomers removed for clarity. The conserved hydrophobic residues around the "chock" are shown in purple. (D) Enlarged view of the "chock" structural element in C. (E) Effects of α -SNAP mutations on the SNARE complex disassembly (upper panel) or on the α-SNAP-dependent binding of NSF to the SNARE complex (lower panel). (F) Histogram of the band intensity relative to the wild type as shown in E.

interacting area with the SNARE helical bundle grooves, which has never been observed before. This interacting region of α -SNAP located on the tip of $\alpha 9/\alpha 10$ helix hairpin forms a chock-like structure squeezing between the two adjacent helical strands of the SNARE four-helix bundle (Figure 3C and 3D, and Supplementary information, Figure S5B). Since the variation of the radii values of the SNARE bundle in the α -SNAP-SNARE complex along the super-helical axis shows a slight difference from that reported from its crystal structure (PDB ID: 1SFC) [3], we estimated that the contact region between the chock and the SNARE bundle is around the layers -2/-3 of the SNARE complex (Supplementary information, Figure S5B). Three highly conserved hydrophobic residues (L197, L198 and Y200) of α-SNAP are located in this region (Supplementary information, Figure S6), suggesting that they might interact with the hydrophobic core of the SNARE complex and weaken the four-helix bundle interaction. Indeed, when these residues were mutated into alanine or glutamate, α-SNAP-dependent binding activity of SNARE with NSF and the SNARE disassembly activity were both reduced (Figure 3E and 3F). More specifically, all mutant α -SNAPs with mutations of L197 or Y200 were severely defective in the SNARE disassembly activity (<5% of that of wild-type α -SNAP), and L198 mutations were less effective but still apparently impaired SNARE disassembly. In addition, mutations to glutamate exhibited more severe effect than mutations to alanine for both the functions, indicating the requirement of hydrophobicity for the proper function. More importantly, the disassembly of the SNARE complex was more severely impaired than α-SNAP-dependent binding of NSF to the SNARE complex for all the mutations, suggesting a direct role of these residues in the SNARE disassembly.

Discussion

Multiple models regarding SNARE complex disassembly in the 20S particle have been proposed. Some studies suggest that the disassembly of a single SNARE by NSF is a processive process with the consumption of ATP molecules ranging from 10 to 50 [33, 34]. An alternative model suggests that turnover of a single ATP is sufficient to disassemble a SNARE complex, indicating a conformational switch of NSF upon ATP hydrolysis to cause the SNARE disassembly [33]. Our 20S particle was prepared with ADP•AlFx, representing the particle at ATP hydrolysis transition state, before the phosphate is released. In this complex, four α -SNAP molecules assemble into a homogeneous structure around the four-helical bundled SNARE complex with a four-fold symmetry, strongly suggesting the cooperative nature of the SNARE disassembly event.

During the submission of our paper, Zhao et al. [35]

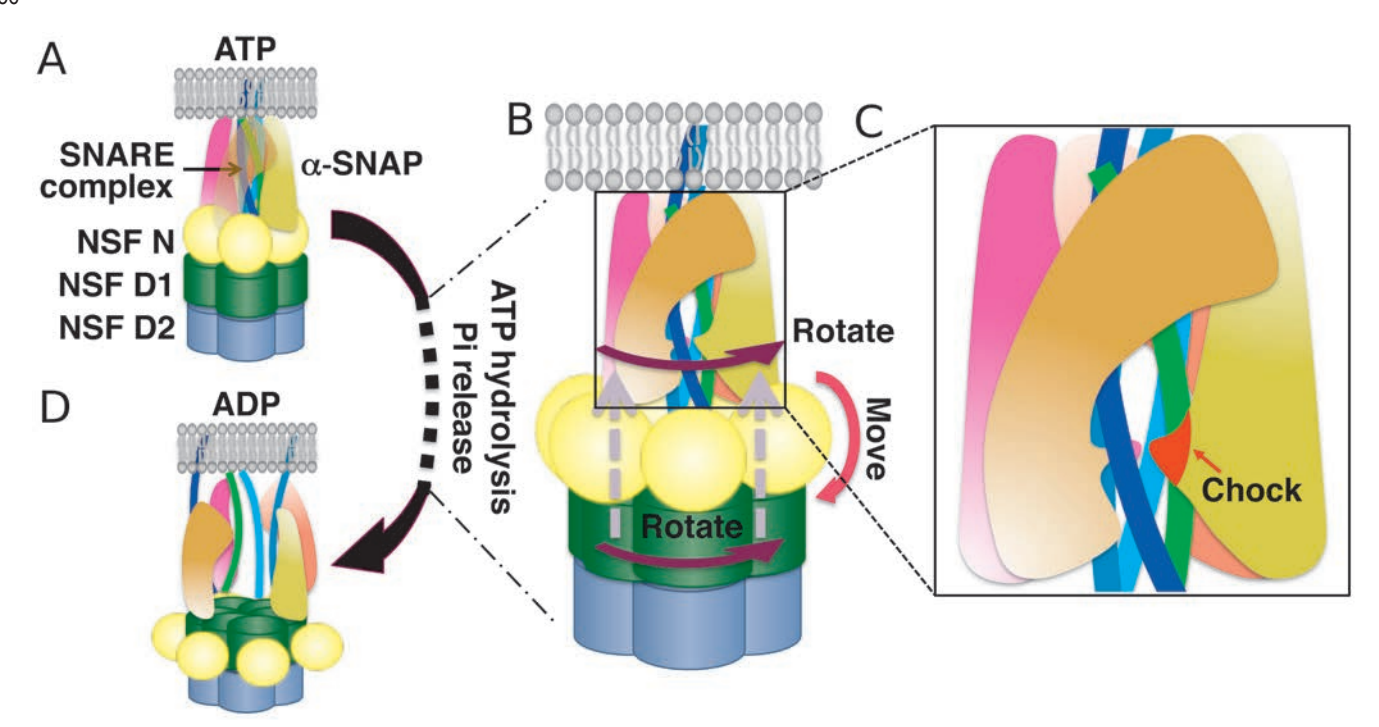


Figure 4 Model of SNARE complex disassembly by the coordinated action of NSF and α -SNAP in a 20S particle. The SNARE complex inserted into the membrane binds to α -SNAPs and NSF to form the 20S particle in the presence of ATP (**A**). During the ATP hydrolysis, the NSF D1 ring rotates counter-clockwise from the top view, which might induce a rotation of the tetrameric α -SNAP assembly in the same direction, and the up-to-down motion of the NSF N-domain might cause α -SNAP to move accordingly (**B**). These two types of movement may lead to the sliding of the "chock" structure along the groove of the SNARE complex (**C**), thus disassembling the SNARE complex after phosphate release (**D**).

reported the architecture of the whole 20S particle at subnanometer resolution with four different global assembly states revealed by 3D classification. In contrast, we used a particle segmentation approach, which allowed us to focus only on the α -SNAP-SNARE assembly in the 20S particle with more detailed information revealed even without classification. This is because the segmentation approach allows the mismatched portions to be reconstructed separately, thus avoiding a major heterogeneity obstacle. Using this approach, the α -SNAP-SNARE assembly was determined to have a four-fold symmetry in the α -SNAP barrel and a pseudo four-fold symmetry in the SNARE bundle, which was also revealed in the paper by Zhao *et al.* [35].

In our reconstruction, a hydrophobic "chock" structure was discovered in the α -SNAP-SNARE assembly. The four-fold symmetrical assembly poises the "chock" of each α -SNAP simultaneously at the same layer of the SNARE four-helix bundle and thus probably generates a localized weak point on the complex ready for breaking apart. We previously solved the structures of NSF hexameric complexes under ADP•AlFx and ADP states and showed that, from the top view, D1 ring rotates \sim

22 degrees counter-clockwise in respective to D2 ring upon the phosphate release [17] (Supplementary information, Figure S7). We also showed that the N-domains of NSFs move to the periphery of the complex when ATP is hydrolyzed to ADP. As the C-terminal domain of α-SNAP interacts directly with the N-domain of NSF [19-23], the movement of the N-domain in the 20S particle very likely causes the similar movement of α -SNAP. It is therefore plausible that, within an assembled 20S particle, a conformational change of the NSF triggered by ATP hydrolysis would be transduced to the tetrameric α-SNAP for it to unwind the SNARE complex (Figure 4). The counter-clockwise rotation of D1 ring might induce a rotation of the α -SNAP assembly in the same direction, while the outwards and downwards motion of the NSF N-domain might cause α -SNAP to move accordingly. A combination of these two types of movement may cause the "chock" structure to slide along the groove of the SNARE complex, thus melting several layers of the structure and exposing them to solvent. This may lead a dramatic disassembly of the SNARE complex as predicted previously [3]. The outwards moving of the NSF N-domain may also serve to pull α-SNAP apart, lead-



ing to a full disassembly of the entire 20S particle. The symmetry mismatch between the tetrameric α -SNAP-SNARE assembly and the hexameric NSF assembly is likely responsible for the mild tilting between these two parts and might actually cause more effective SNARE complex melting by snapping its very N-terminal region within the D1 domain.

Materials and Methods

Protein expression and purification

Chinese hamster ovary NSF, *Bos Taurus* α -SNAP, and *Rattus norvegicus* SNARE proteins syntaxin 2-253, soluble VAMP 1-94, SNAP-25 1-100, SNAP-25 125-206 were expressed and purified as previously described [17]. Full-length VAMP 1-116 with a transmembrane domain was purified in the same way as soluble VAMP 1-94 with a modification of 1% (w/v) of octyl glucopyranoside (OG) included in the buffer. MSP1D1 was expressed and purified as described before [30]. The site-directed mutants of α -SNAP were generated with overlap PCR and cloned into the pGEX-4T-1 vector. All of the mutations were confirmed by DNA sequencing. Mutated proteins were expressed and purified as the wild-type α -SNAP protein. The purity and quality of all the purified proteins were verified by SDS-PAGE.

SNARE complex reconstitution and disassembly by NSF

Soluble SNARE complex was reconstituted by incubating SNARE proteins (syntaxin 2-253, soluble VAMP 1-94, SNAP-25 1-100 and SNAP-25 125-206) in an equal molar concentration in the reconstitution buffer (50 mM HEPES-NaOH, 100 mM NaCl, 1 mM DTT, pH 7.6) overnight at 4 °C. Its formation was confirmed by SDS-PAGE. SNARE complex was separated from individual SNARE proteins by sequential affinity chromatography with glutathione agarose beads (GE Healthcare) and Ni²⁺-NTA beads (Qiagen). Then the SNARE complex was incubated with thrombin (2 U/ml) overnight at 4 °C to cleave the GST tag and His tag. The resulted complex was further purified by gel filtration chromatography using a Superdex 200 10/30GL column (GE Healthcare).

For SNARE complex disassembly assay, NSF was mixed with an appropriate amount of $\alpha\textsc{-SNAP}$ and SNARE complex in the reconstitution buffer. ATP plus MgCl $_2$ or EDTA was then added to a final concentration of 2 mM each. The mixture was incubated for 40 min at 37 °C, and then SDS-PAGE loading buffer was added to stop the reaction. The samples were then subjected to SDS-PAGE analysis without heating.

Preparation of 20S particle in NP40-containing solution

Soluble SNARE complex, NSF hexamer and α-SNAP (3:1:15 molar ratio) were incubated in the reconstitution buffer containing 0.1% (v/v) NP40, 2 mM ADP•AlFx and 2 mM MgCl₂ overnight at 4 °C. The assembled 20S particle was separated from unassembled components and purified by gel filtration chromatography using a Superdex 200 HiLoad column (GE Healthcare) in the reconstitution buffer containing 2 mM MgCl₂.

Preparation of nanodisc-20S particle

The palmitoyl-2-oleoyl phosphatidylcholine:1,2-dioleoyl phosphatidylserine:1,2-dipalmitoyl phosphatidylethanolamine =

82:15:3 (Avanti Polar Lipids) lipid mixture dissolved in chloroform was dried in a glass tube under gentle nitrogen flow followed by vacuum drying for 4 h to overnight. The lipid film was then suspended in the reconstitution buffer to the final concentration of 5-20 mM. Then the MSP1D1 and SNARE complex containing full-length VAMP as well as 1% OG were added. To ensure only one SNARE complex per nanodisc, the protein/lipid ratio was SNARE complex:MSP1D1: lipid = 0.2:2:120, according to the previous report [31]. We then vortexed and ultra-sonicated the mixture using an ultrasonic cleaner (KQ-50E, Kunshan Shumei Company, China; 50 W, 40 KHz) at room temperature for 20 min followed by 3-h shaking at 4 °C. SM-2 bio-beads were then added into the mixture to 0.5-0.8 g/ml, which was then shaken overnight to remove the detergent. The bio-beads were removed by centrifugation of the solution and the nanodisc-SNARE complex was purified by gel filtration using a Superdex 200 column (GE Healthcare) in the reconstitution buffer.

To obtain the nanodisc-20S, the nanodisc-SNARE complex, NSF hexamer and $\alpha\text{-SNAP}$ (3:1:15 molar ratio) were incubated in the reconstitution buffer with 2 mM ADP•AlFx and 2 mM MgCl $_2$ overnight at 4 °C. The successfully assembled nanodisc-20S particle was separated from the other components and purified by gel filtration using a Superose 6 column (GE Healthcare) in the reconstitution buffer containing 2 mM MgCl $_2$. Sample fractions were concentrated by Amicon ultra (0.5 ml, 30 kD cutoff) centrifugal filter units if necessary.

Negative staining EM

A drop of 4 μl of 20S or nanodisc-20S sample (~0.1 μM) was applied to a glow-discharged copper grid coated with a continuous carbon film, and then stained with 2% (w/v) uranyl acetate for 1 min. Digitized images of negatively stained protein were collected using an FEI Tecnai-12 transmission electron microscope operated at 120 kV and nominal magnification of 68 000 equipped with a Gatan UltraScan4000 CCD camera, with an equivalent pixel size of 1.6 Å at the specimen level. A total of 300 micrographs of nanodisc-20S particles were recorded from which 15 076 particles were boxed using e2boxer.py in EMAN2 [36]. Using our previous reconstruction of the 20S particle [17] low-pass filtered to 80 Å resolution, we performed 3D reconstruction of the negatively stained nanodisc-20S particles by EMAN2 without any symmetry imposition.

Cryo-EM and data collection

A droplet of 4 µl of 20S or nanodisc-20S sample (~5 µM) was applied to glow-discharged Quantifoil R1.2/1.3 holey carbon grids (Quantifoil Micro Tools GmbH), blotted for 1 s, and plunge-frozen by using FEI Vitrobot Mark IV. An additional continuous ultra-thin carbon film was covered on the holey grids before nanodisc-20S sample loading in order to get more particles inside hole. The grids were imaged with FEI Titan Krios equipped with K2 Summit electron counting camera (Gatan) operated at 300 kV and nominal magnification of 22 500× corresponding to a physical pixel size of 1.32 Å at the specimen level. Total 2 349 movie stacks of nanodisc-20S and 847 movie stacks of 20S were manually collected with UCSF-Image4 [37]. The electron dose rate was set to 8 counts/physical pixel/s (~10 e⁻/physical pixel/s). Each stack was dose-fractionated to 32 frames with 0.25 s frame exposure and totally 8-s exposure (a total dose of 46 electron/Å² on the specimen).



All stacks were recorded with super-resolution mode of K2 camera and motion was corrected with 2× binning option as described previously [37]. The pixel size of final motion-corrected micrographs was 1.32 Å/pixel.

Data processing

For the autopicking of 20S particles, 12 584 20S particles were boxed from 94 micrographs using e2boxer.py in EMAN2 [36]. Then the boxed particles were extracted from micrographs and 2D classified using RELION 1.3 [38, 39]. The defocus values of micrographs were estimated using CTFFIND3 [40]. The generated 2D class averages were used as the templates for the subsequent autopicking of 20S particles. The autopicking of ND-20S particles was the same as that of the 20S particles, with the 2D class averages from 9 825 ND-20S particles from 80 micrographs. Total 165 401 20S particles and 299 135 nanodisc-20S particles were automatically picked out and 2D classified using RELION 1.3 [41]. The 2D class averages of 20S showed mainly top views, while mainly side views were observed in the 2D class averages of ND-20S. 201 054 ND-20S particles were empirically selected from good classes of 2D classifications, and then subjected to 3D classification and refinement without symmetry using RELION1.3 [38, 39]. The previous 3D reconstruction map of negatively stained ND-20S was used as an initial model. A tilt angle restriction from 60 to 120° was imposed during the 3D classification and refinement. A reconstruction of the entire 20S particle was reconstructed at a resolution of 13 Å by this means. To further improve the refinement accuracy of the upper part composed of the α-SNAP-SNARE assembly, we segmented the D1-D2 density from the 13 Å resolution map, generated the reprojection of it in a corresponding view of every raw particle image of the ND-20S particle, and subtracted the reprojection from the raw particle image using a home-modified program in RELION (Supplementary information, Figure S3). The subtraction-resulted particles were then centered and re-windowed for the upper part of the 20S particle to serve as a new data set for 2D classification and 3D reconstruction. The class averages calculated from these particle images together with the top view 2D class averages of the 20S particle were used to generate an initial model by EMAN2 with C4 symmetry (the symmetry was determined as described in Supplementary information, Figures S1F and S4H). The following 3D classification and refinement were performed with C4 symmetry imposed using RELION 1.3 [38, 39]. The final 3D reconstruction was calculated from 64 710 upper particles. Its resolution was determined as 7.35 Å based on the gold-standard Fourier shell correlation (FSC) 0.143 criterion [42], where the high-resolution noise substitution approach [43] was used to correct the FSC curve.

Atomic model docking

A homology atomic model of α -SNAP from *Bos Taurus* was built with Modeller [44, 45] using the crystal structure of α -SNAP from *Saccharomyces cerevisiae* (PDB ID: 1QQE) as reference model. The crystal structrue of SNARE complex (PDB ID: 1SFC) and the atomic model of α -SNAP built above were docked as rigid body into the cryo-EM map of the reconstruction from upper portion of nandisc-20S particles by UCSF Chimera [46].

α-SNAP-dependent binding of NSF to MBP-SNARE assay and MBP-SNARE disassembly assay

The α -SNAP-dependent binding of NSF to SNARE assay was performed as described before [47]. For MBP-SNARE disassembly assay, MBP-SNARE complexes were incubated with NSF, and wild-type or mutant α -SNAP proteins or without α -SNAP in the presence of Mg²+-ATP at 37 °C for 30 min, followed by the addition of SDS-PAGE sample buffer to stop the reactions and analyzed by SDS-PAGE. The gels were then stained with Coomassie blue and the MBP-SNARE proteins were quantified by densitometry using ImageJ [48]. The MBP-SNARE disassembly activities of wild-type and mutant α -SNAP at 30 min were averaged from three independent measurements and calculated as follows: disassembled protein, obtained by subtracting remaining protein (30 min) from total protein (without α -SNAP), divided by total protein. Values were normalized to that of wild-type α -SNAP. Error bars indicate the deviations.

Data deposition

The density map of α -SNAP-SNARE assembly has been deposited in Electron Microscopy Data Bank (www.emdatabank. org; EMDB ID code: 2874).

Acknowledgments

We are grateful to Chapman ER (University of Wisconsin, Madison) for providing plasmids encoding VAMP 1-94, VAMP 1-116, SNAP-25 1-100, SNAP-25 125-206, NSF and α-SNAP, Rizo J (University of Texas Southwestern Medical Center) for providing plasmids encoding syntaxin 2-253, and Rothman J (Yale University) for providing plasmid encoding MSP1D1. We thank Lei JL and Xu Y for the EM support, Yang T and Wang Y for computer support, and Xie J for her excellent technical support. We acknowledge the Tsinghua University Branch of China National Center for Protein Sciences Beijing and the "Explorer 100" cluster system of the Tsinghua National Laboratory for Information Science and Technology for providing EM and computation resources. This work was supported by the National Basic Research Program of China (2011CB910500 and 2012CB917303) and the National Natural Science Foundation of China (31230016, 31370717 and 31400632). QZ was supported by the Postdoctoral Fellowship of Tsinghua-Peking Joint Center for Life Sciences.

References

- Söllner T, Whiteheart SW, Brunner M, et al. SNAP receptors implicated in vesicle targeting and fusion. Nature 1993; 362:318-324.
- 2 Rothman JE. Mechanisms of intracellular protein transport. Nature 1994; 372:55-63.
- 3 Sutton RB, Fasshauer D, Jahn R, Brunger AT. Crystal structure of a SNARE complex involved in synaptic exocytosis at 2.4 Å resolution. *Nature* 1998; **395**:347-353.
- 4 Antonin W, Fasshauer D, Becker S, Jahn R, Schneider TR. Crystal structure of the endosomal SNARE complex reveals common structural principles of all SNAREs. *Nat Struct Biol* 2002; 9:107-111.
- 5 Jahn R, Scheller RH. SNAREs--engines for membrane fusion. Nat Rev Mol Cell Biol 2006; 7:631-643.
- 6 Stein A, Weber G, Wahl MC, Jahn R. Helical extension of the neuronal SNARE complex into the membrane. *Nature* 2009;



- 460:525-528.
- 7 Weber T, Zemelman BV, McNew JA, et al. SNAREpins: minimal machinery for membrane fusion. Cell 1998; 92:759-772.
- Ungar D, Hughson FM. SNARE protein structure and function. Annu Rev Cell Dev Biol 2003; 19:493-517.
- Wilson DW, Whiteheart SW, Wiedmann M, Brunner M, Rothman JE. A multisubunit particle implicated in membrane fusion. J Cell Biol 1992; 117:531-538.
- 10 Söllner T, Bennett MK, Whiteheart SW, Scheller RH, Rothman JE. A protein assembly-disassembly pathway in vitro that may correspond to sequential steps of synaptic vesicle docking, activation, and fusion. Cell 1993; 75:409-418.
- Mayer A, Wickner W, Haas A. Sec18p (NSF)-driven release of Sec17p (alpha-SNAP) can precede docking and fusion of yeast vacuoles. Cell 1996; 85:83-94.
- Hayashi T, Yamasaki S, Nauenburg S, Binz T, Niemann H. Disassembly of the reconstituted synaptic vesicle membrane fusion complex in vitro. EMBO J 1995; 14:2317-2325.
- Tagaya M, Wilson DW, Brunner M, Arango N, Rothman JE. Domain structure of an N-ethylmaleimide-sensitive fusion protein involved in vesicular transport. J Biol Chem 1993; **268**:2662.
- 14 Fleming KG, Hohl TM, Yu RC, et al. A revised model for the oligomeric state of the N-ethylmaleimide-sensitive fusion protein, NSF. J Biol Chem 1998; 273:15675-15681.
- 15 Zhao C, Smith EC, Whiteheart SW. Requirements for the catalytic cycle of the N-ethylmaleimide-Sensitive Factor (NSF). Biochim Biophys Acta 2012; 1823:159-171.
- Nagiec EE, Bernstein A, Whiteheart SW. Each domain of the N-ethylmaleimide-sensitive fusion protein contributes to its transport activity. J Biol Chem 1995; 270:29182-29188.
- Chang LF, Chen S, Liu CC, et al. Structural characterization of full-length NSF and 20S particles. Nat Struct Mol Biol 2012: 19:268-275.
- 18 Moeller A, Zhao C, Fried MG, Wilson-Kubalek EM, Carragher B, Whiteheart SW. Nucleotide-dependent conformational changes in the N-Ethylmaleimide Sensitive Factor (NSF) and their potential role in SNARE complex disassembly. J Struct Biol 2012; 177:335-343.
- Weidman PJ, Melançon P, Block MR, Rothman JE. Binding of an N-ethylmaleimide-sensitive fusion protein to Golgi membranes requires both a soluble protein(s) and an integral membrane receptor. J Cell Biol 1989; 108:1589-1596.
- Barnard RJ, Morgan A, Burgoyne RD. Domains of alpha-SNAP required for the stimulation of exocytosis and for N-ethylmalemide-sensitive fusion protein (NSF) binding and activation. Mol Biol Cell 1996; 7:693-701.
- May AP, Misura KM, Whiteheart SW, Weis WI. Crystal structure of the amino-terminal domain of N-ethylmaleimide-sensitive fusion protein. Nat Cell Biol 1999; 1:175-182.
- Yu RC, Jahn R, Brunger AT. NSF N-terminal domain crystal structure: models of NSF function. Mol Cell 1999; 4:97-107.
- Matveeva EA, May AP, He P, Whiteheart SW. Uncoupling the ATPase activity of the N-ethylmaleimide sensitive factor (NSF) from 20S complex disassembly. Biochemistry 2002; 41:530-536.
- Rice LM, Brunger AT. Crystal structure of the vesicular transport protein Sec17: implications for SNAP function in SNARE complex disassembly. Mol Cell 1999; 4:85-95.

- 25 Marz KE, Lauer JM, Hanson PI. Defining the SNARE complex binding surface of alpha-SNAP: implications for SNARE complex disassembly. J Biol Chem 2003: 278:27000-27008.
- Hohl TM, Parlati F, Wimmer C, Rothman JE, Sollner TH, Engelhardt H. Arrangement of subunits in 20S particles consisting of NSF, SNAPs, and SNARE complexes. Mol Cell 1998; 2:539-548.
- 27 Owen DJ, Schiavo G. A handle on NSF. Nat Cell Biol. 1999 1:E127-E128.
- 28 Wimmer C, Hohl TM, Hughes CA, et al. Molecular mass, stoichiometry, and assembly of 20S particles. J Biol Chem 2001; 276:29091-29097.
- Denisov IG, Grinkova YV, Lazarides AA, Sligar SG. Directed self-assembly of monodisperse phospholipid bilayer Nanodiscs with controlled size. J Am Chem Soc 2004; 126:3477-3487.
- 30 Ritchie TK, Grinkova YV, Bayburt TH, et al. Chapter 11 -Reconstitution of membrane proteins in phospholipid bilayer nanodiscs. Methods Enzymol 2009; 464:211-231.
- Shi L, Shen OT, Kiel A, et al. SNARE proteins: one to fuse and three to keep the nascent fusion pore open. Science 2012; **335**:1355-1359.
- Shi L, Howan K, Shen QT, Wang YJ, Rothman JE, Pincet F. Preparation and characterization of SNARE-containing nanodiscs and direct study of cargo release through fusion pores. Nat Protoc 2013; 8:935-948.
- 33 Cipriano DJ, Jung J, Vivona S, Fenn TD, Brunger AT, Bryant Z. Processive ATP-driven substrate disassembly by the N-Ethylmaleimide-sensitive Factor (NSF) molecular machine. J Biol Chem 2013; 288:23436-23445.
- Shah N, Colbert KN, Enos MD, Herschlag D, Weis WI. Three αSNAP and 10 ATP molecules are used in SNARE complex disassembly by N-ethylmaleimide-sensitive Factor (NSF). J Biol Chem 2015; 290:2175-2188.
- Zhao M, Wu S, Zhou Q, et al. Mechanistic insights into the recycling machine of the SNARE complex. Nature 2015; **518**:61-67.
- Tang G, Peng L, Baldwin PR, et al. EMAN2: an extensible image processing suite for electron microscopy. J Struct Biol 2007; 157:38-46.
- Li X, Mooney P, Zheng S, et al. Electron counting and beam-induced motion correction enable near-atomic-resolution single-particle cryo-EM. Nat Methods 2013; 10:584-590.
- 38 Scheres SH. A Bayesian view on cryo-EM structure determination. J Mol Biol 2012; 415:406-418.
- Scheres SH. RELION: implementation of a Bayesian approach to cryo-EM structure determination. J Struct Biol 2012; 180:519-530.
- 40 Mindell JA, Grigorieff N. Accurate determination of local defocus and specimen tilt in electron microscopy. J Struct Biol 2003; 142:334-347.
- 41 Scheres SHW. Semi-automated selection of cryo-EM particles in RELION-1.3. J Struct Biol 2015; 189:114-122.
- Scheres SHW, Chen S. Prevention of overfitting in cryo-EM structure determination. Nat Methods 2012; 9:853-854.
- Chen S, McMullan G, Faruqi AR, et al. High-resolution noise substitution to measure overfitting and validate resolution in 3D structure determination by single particle electron cryomicroscopy. Ultramicroscopy 2013; 135:24-35.



- 44 Sali A, Blundell TL. Comparative protein modelling by satisfaction of spatial restraints. J Mol Biol 1993; 234:779-815.
- 45 Webb B, Sali A. Comparative protein structure modeling using MODELLER. Curr Protoc Bioinformatics 2014; 47:5.6.1-5.6.32.
- 46 Pettersen EF, Goddard TD, Huang CC, et al. UCSF Chimera - a visualization system for exploratory research and analy-
- sis. J Comput Chem 2004; 25:1605-1612.
- 47 Liu CC, Sun S, Sui SF. The role of the N-D1 linker of the N-ethylmaleimide-sensitive factor in the SNARE disassembly. PLoS One 2013; 8:e64346.
- 48 Schneider CA, Rasband WS, Eliceiri KW. NIH Image to ImageJ: 25 years of image analysis. Nat Methods 2012; 9:671-675.

(Supplementary information is linked to the online version of the paper on the Cell Research website.)